International Journal for Multiscale Computational Engineering, 1(1)115–126 (2003)

Coupling Methods for Continuum Model with Molecular Model

T. Belytschko[1] *& S. P. Xiao*[2]

Department of Mechanical Engineering, 2145 N, Sheridan Rd., Northwestern University, Evanston, IL 60208

ABSTRACT

This article develops coupling methods for continuum models with molecular models. Two methods are studied here: an overlapping domain decomposition method, which has overlapping domain; and an edge-to-edge decomposition method, which has an interface between the two models. These two methods enforce compatibility on the overlapping domain or interface nodes/atoms by the Lagrange multiplier method or the augmented Lagrangian method.

[1] Walter P Murphy Professor of Mechanical Engineering
[2] Post Doctorate, Mechanical Engineering

Document ID# JMC0101-115–126(008)
0731-8898/03/$5.00

1. INTRODUCTION

In the analysis of phenomena at the molecular level, it is often desirable to deal with much larger models than can conveniently be treated entirely with molecular mechanics. For example, in studying fracture, a rather large subdomain around the crack needs to be modeled in order to obtain the correct compliance; or, in the case of dynamics, the correct impedance around the area needs to be modeled by molecular mechanics. This then entails coupling the molecular mechanics model with a continuum model. Coupling subdomains is an area that has been extensively developed over the past two decades; the corresponding methods are called *domain decomposition* methods. Coupling molecular models with continuum models is somewhat different, because the character of the models differs; this has come to be called heterogeneous domain decomposition.

Because molecular models are essential for such phenomena as the rearrangement of bonds but are more expensive than continuum models, coupled methods are attractive. Molecular models [1] usually contain millions of atoms for a microscale system, and, consequently, they are also very expensive. The continuum/finite element approach [2] dramatically reduces the computational time but does not have the ability to represent the details of bonds or atoms.

In this article, methods for coupling continuum models with molecular models are developed for large deformations of nanosystems, with a focus on nanotubes. The methodology is based on domain decomposition, which was developed in the early eighties and is widely used for the numerical solution of partial differential equations [3, 4]. Two approaches are considered here: domain decomposition with overlapping domains, recently often called "handshake" models in physics literature (e.g. Abraham et al. [5]), and the edge-to-edge decomposition method. Domain decompositions were also applied to discretization methods such as finite difference or finite element methods, particularly for the parallel implementation of the finite element method [6, 7] and the coupling methods of BEM (boundary element method) with FEM [8, 9].

The outline of this article is as follows. Section 2 briefly introduces the governing equations for the continuum model and molecular. Sections 3 and 4 develop the two coupling methods under discussion. Section 5 gives four examples to examine the accuracy of these coupling methods.

2. GOVERNING EQUATIONS

2.1. Continuum Equations

The physical principles governing the continuum are the conservation of mass, momentum, and energy. We consider a Lagrangian description under adiabatic conditions, so conservation of mass is an algebraic equation and conservation of energy is an ordinary differential equation (ODE) for the energy (see Belytschko et al. [10]). We employ a so-called "total Lagrangian" description, so the linear momentum equations are

$$\frac{\partial \mathbf{P}_{ji}}{\partial X_j} + \rho_0 \mathbf{b}_i = \rho_0 \ddot{\mathbf{u}}_i \tag{1}$$

where ρ_0 is the initial density, $\mathbf{P}$ is the nominal stress tensor, $\mathbf{b}$ is the body force per unit mass, $\mathbf{u}$ is the displacement, and the superposed dots denote material time derivatives. These momentum equations are simply transformations of the better-known equations in terms of the Cauchy stress and current coordinates, so this choice does not limit the methods.

The weak form of the momentum conservation equation is

$$\int_{\Omega_0} \delta u_i \rho_0 \ddot{u}_i d\Omega_0 = \int_{\Omega_0} \delta u_i \rho_0 b_i d\Omega_0 - \int_{\Omega_0} \delta F_{ij} P_{ji} d\Omega_0 + \int_{\Gamma_0} \delta u_i \bar{t}_i d\Gamma_0 \tag{2}$$

where Ω_0 is the reference configuration, δu_i is the test function, and $\bar{t}_i$ is the prescribed boundary traction. By using an approximation

$$\mathbf{u}(\mathbf{X},t) = \sum_I N_I(\mathbf{X})\mathbf{u}_I(t) \quad \text{or}$$

$$u_i(\mathbf{X},t) = \sum_I N_I(\mathbf{X}) u_{iI}(t) \tag{3}$$

where $N_I(\mathbf{X})$ are the shape functions and a similar expansion for $\delta\mathbf{u}(\mathbf{X})$, the following discrete equations are obtained:

$$m_I \ddot{u}_{iI} = f_{iI}^{ext} - f_{iI}^{int} \qquad m_I = \rho_0 V_I^o \tag{4}$$

where f_{iI}^{ext} and f_{iI}^{int} are the external and internal nodal forces, respectively, given by

$$f_{iI}^{ext} = \int_{\Omega_0} \rho_0 N_I b_i d\Omega_0 + \int_{\Gamma_0'} N_I \bar{t}_i d\Gamma_0 \tag{5}$$

$$f_{iI}^{\text{int}} = \int_{\Omega_0} \frac{\partial N_I(\mathbf{X})}{\partial X_j} P_{ji} d\Omega_0 = \int_{\Omega} \frac{\partial N_I(\mathbf{x})}{\partial x_j} \sigma_{ji} d\Omega \tag{6}$$

and Ω is the current domain (see Belytschko et al. [10] for details).

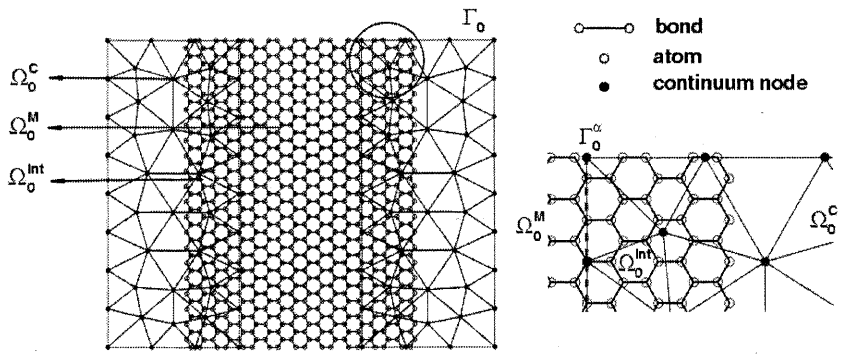

FIGURE 1. Overlapping domain decomposition method.

2.2. Molecular Mechanics

Consider a set of n_M molecules with the initial coordinates $\mathbf{X}_I$, $I = 1$ to n_M. Let the displacements be denoted by $\mathbf{d}_I(t)$. The potential energy is given by $W_M(\mathbf{d})$. For a given potential function $W_M(\mathbf{d})$, an equilibrium state is given by

$$dW_M(\mathbf{d}) = 0 \tag{7}$$

3. COUPLING METHOD I: OVERLAPPING DOMAIN DECOMPOSITION

3.1. Coupling Model

In developing this coupling procedure for the continuum model with molecular model, we have several aims.

1. The procedure should be able to treat large deformations and be applicable to circumstances where atoms emerge from the coupling region.

2. The constraints between the atoms and the continuum should be developed in a manner consistent with the overall potential.

The resulting coupling method is similar to the handshake methods developed by Abraham et al. [5]. The main features are

1. A Lagrange multiplier method and an augmented Lagrangian method are used to apply the constraints on the motion.

2. The Lagrange multiplier field in the overlapping domain vanishes at the edge of the continuum domain so that the interaction forces between the continuum and molecular mechanics model are smooth if an atom exits the overlapping domain.

We denote the complete domain in the initial configuration by Ω_0 and its boundaries by Γ_0; Γ_0 consists of traction boundaries Γ_0^t and the displacement boundaries Γ_0^u. The domain is subdivided into the subdomains treated by continuum mechanics, Ω_0^C, and that treated by molecular mechanics, Ω_0^M; the latter is the domain encompassed by the atoms of the model. The intersection of these two domains is denoted by Ω_0^{int} in the initial configuration and by Ω^{int} in the current configuration (Ω^{int} is often called the handshake domain); Γ_0^α denotes the edges of the continuum domain. An example of a model is shown in Fig. 1.

The potential energy of the bond I–J is denoted by $w_{IJ} = w_M(\mathbf{x}_I, \mathbf{x}_J)$, where $\mathbf{x}_I = \mathbf{X}_I + \mathbf{d}_I$ is the current position of atom I. The total potential energy of the molecular mechanics subdomain Ω^M is then

$$W_M^{int} = \frac{1}{2}\sum_I \sum_J w_M(\mathbf{x}_I, \mathbf{x}_J) \tag{8}$$

The potential energy per unit volume of the continuum is denoted by $w_C(\mathbf{F})$ and the total potential energy of the continuum is given by

$$W_C^{\text{int}} = \int_{\Omega_0^C} \rho_0 w_C(\mathbf{F}) d\Omega_0^C \tag{9}$$

In expressing the total internal potential energy of the system, we employ a scaling parameter α in the intersection subdomain. The parameter α is defined as $\alpha = [l(\mathbf{X}) / l_0]$, where $l(\mathbf{X})$ is the least square projection of $\mathbf{X}$ onto Γ_0^α, as shown in Fig. 2. The scaling parameter vanishes at the edge of the continuum and is unity at the other edge of Ω_0^{int}; it is important that Ω_0^{int} includes the last line of atoms.

Therefore, the total potential energy is given by

$$W^{\text{int}} = \int_{\Omega_0^C} \beta^C(\mathbf{X})\rho_0 w_C(\mathbf{F}) d\Omega_0^C + \frac{1}{2}\sum_I \sum_J \beta^M(\mathbf{X}_I) w_M(\mathbf{x}_I, \mathbf{x}_J) \tag{10}$$

and the internal forces are

$$\mathbf{F}_J^{\text{int}} = \int_{\Omega_0^C} \beta^C(\mathbf{X})\rho_0 \frac{\partial w_C(\mathbf{F})}{\partial \mathbf{u}_J} d\Omega_0^C$$

$$\mathbf{f}_J^{\text{int}} = \frac{1}{2}\sum_I \sum_J \beta^M(\mathbf{X}_I) \frac{\partial w_M(\mathbf{x}_I, \mathbf{x}_J)}{\partial \mathbf{d}_J} \tag{11}$$

where the scaling field β is defined as

$$\beta^C(\mathbf{X}) = \begin{cases} 0 & in \quad \Omega_0^M \\ \alpha & in \quad \Omega_0^{int} \\ 1 & in \quad \Omega_0^C - \Omega_0^{\text{int}} \end{cases}$$

$$\beta^M(\mathbf{X}) = \begin{cases} 0 & in \quad \Omega_0^C \\ 1-\alpha & in \quad \Omega_0^{\text{int}} \\ 1 & in \quad \Omega_0^M - \Omega_0^{int} \end{cases}$$

The external potential is scaled similarly, so

$$W^{\text{ext}} = \int_{\Omega_0^C} \beta^C(\mathbf{X})\rho_0 \mathbf{b}\cdot\mathbf{u} d\Omega_0^C + \int_{\Gamma_0^t} \beta^C(\mathbf{X})\rho_0 \bar{\mathbf{t}}\cdot\mathbf{u} d\Gamma_0^t + \sum_I \beta^M(\mathbf{X}_I)\bar{\mathbf{f}}_I^{\text{ext}}\cdot\mathbf{d}_I \tag{12}$$

where $\bar{\mathbf{f}}_I^{\text{ext}}$ is any external force applied to atom I. Note that the above linear combination gives the correct total external and internal potential of the model.

The two models are constrained on the overlapping region Ω_0^{int} by

$$g_I = \left\|\mathbf{u}(\mathbf{X}_I) - \mathbf{d}_I\right\|^2 = \sum_i \left[u_i(\mathbf{X}_I) - d_{iI}\right]^2 = 0 \tag{13}$$

i.e., the continuum displacements conform to the atomic displacements at the discrete positions of the atoms. A single constraint is applied, rather than imposing the constraint on each component of the displacement, because this single constraint suffices to enforce displacement continuity. We first show how the constraint is applied by the Lagrange multiplier method; we then add the modifications needed for the augmented Lagrangian method, which provides a better numerical method.

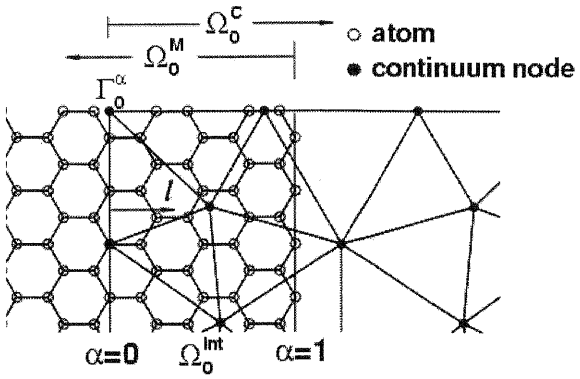

FIGURE 2. Intersection domain between continuum and molecular model.

In the Lagrange multiplier method, the problem can be posed as follows: find the stationary point of

$$W_L = W^{\text{int}} - W^{\text{ext}} + \boldsymbol{\lambda}^T\mathbf{g} \tag{14}$$

where $\boldsymbol{\lambda} = \{\lambda_I\}$ is the vector of Lagrange multipliers for the constraint (13) for each of the atoms.

To develop the corresponding discrete equations, we use a finite element method in Ω_0^C and molecular mechanics in Ω_0^M. The displacements in Ω_0^C are then given in terms of shape functions $N_I(\mathbf{X})$ by

$$\mathbf{u}(\mathbf{X}, t) = \sum_I N_I(\mathbf{X})\mathbf{u}_I(t) \tag{15}$$

The Lagrange multiplier field is also expressed in terms of shape functions denoted by $\Lambda_I(\mathbf{X})$:

$$\lambda(\mathbf{X}, t) = \sum_I \Lambda_I(\mathbf{X})\bar{\lambda}_I(t) \tag{16}$$

Generally, the shape functions for the Lagrange multiplier field will differ from that for the displacement, $N_I(\mathbf{X})$, and they must satisfy the LBB conditions. The Lagrange multiplier field is usually constructed by an auxiliary finite element triangulation of the intersection (overlapping) domain, as shown in Fig. 3. To distinguish the Lagrange multiplier λ_I in Eq. (14) from the nodal values at the field, we use $\bar{\lambda}_I$ to denote the Lagrange multiplier at the Lagrange multiplier nodes.

We define the external nodal forces in the conventional way on the continuum nodes with the same scaling as the internal nodal forces (11) by

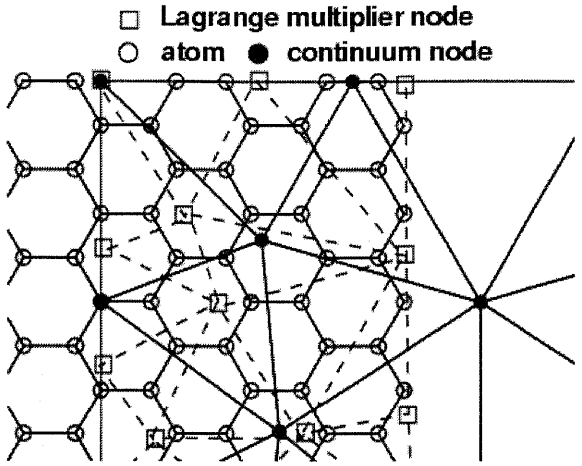

FIGURE 3. Lagrange multiplier interpolation.

$$\mathbf{F}_I^{ext} = \int_{\Omega_0^C} \beta^C(\mathbf{X}) N_I \rho_0 \mathbf{b} d\Omega_0^C + \int_{\Gamma_0^t} \beta^C(\mathbf{X}) N_I \bar{\mathbf{t}} d\Gamma_0^t \tag{17}$$

The external potential (12) can then be written as

$$W^{\text{ext}} = \sum_I \mathbf{F}_I^{\text{ext}} \cdot \mathbf{u}_I + \sum_I \mathbf{f}_I^{\text{ext}} \cdot \mathbf{d}_I \tag{18}$$

where $\mathbf{f}_I^{\text{ext}} = \beta^M(\mathbf{X}_I)\bar{\mathbf{f}}_I^{\text{ext}}$.

The augmented Lagrangian method can be developed by adding a penalty to Eq. (14), as follows:

$$W_{AL} = W^{\text{int}} - W^{\text{ext}} + \boldsymbol{\lambda}^T \mathbf{g} + \frac{1}{2} p \mathbf{g}^T \mathbf{g} \tag{19}$$

where p is the penalty parameter; if $p = 0$, Eq. (19) is identical to Eq. (14).

3.2. Discrete Equations

The discrete equations are then obtained by inserting Eqs. (15) and (16) into Eq. (19) and setting the derivatives of W_{AL} with respect to $\mathbf{u}_I$ (or $\mathbf{d}_I$) and $\bar{\lambda}_I$ to zero. This gives

$$\frac{\partial W_{AL}}{\partial u_{iI}} = (F_{iI}^{\text{int}} - F_{iI}^{\text{ext}}) + 2\sum_L \left[\left(\sum_K \Lambda_{KL} \bar{\lambda}_K \right) \left(\sum_K N_{KL} u_{iK} - d_{iL} \right) N_{IL} \right] + 2p \sum_L \left\{ \begin{bmatrix} \sum_j \left(\sum_K N_{KL} u_{jK} - d_{jL} \right)^2 \end{bmatrix} + \left(\sum_K N_{KL} u_{iK} - d_{iL} \right) N_{IL} \right\} = 0 \tag{20}$$

$$\frac{\partial W_{AL}}{\partial d_{iI}} = (f_{iI}^{\text{int}} - f_{iI}^{ext}) - 2\left(\sum_K \Lambda_{KI} \bar{\lambda}_K \right) \left(\sum_K N_{KI} u_{iK} - d_{iI} \right) - 2p \left[\sum_j \left(\sum_K N_{KI} u_{jK} - d_{jI} \right)^2 \right] \left(\sum_K N_{KI} u_{iK} - d_{iI} \right) = 0 \tag{21}$$

$$\frac{\partial W_{AL}}{\partial \bar{\lambda}_I} = \sum_L \Lambda_{IL} \left(\sum_K \sum_i (N_{KL} u_{iK} - d_{iL})^2 \right) = 0 \tag{22}$$

where $N_{KI} = N_K(\mathbf{X}_I)$, $\Lambda_{KI} = \Lambda_K(\mathbf{X}_I)$.

For Newton methods, the increments in the internal nodal force are related to the increments in the nodal displacement by Jacobian or stiffness matrices:

$$\Delta \mathbf{F}_I^{\text{int}} = \sum_J \mathbf{K}_{IJ}^C \Delta \mathbf{u}_J \quad \text{or} \quad \Delta \mathbf{F}^{\text{int}} = \mathbf{K}^C \Delta \mathbf{d}^C \tag{23}$$

$$\Delta \mathbf{f}_I^{\text{int}} = \sum_J \mathbf{K}_{IJ}^M \Delta \mathbf{d}_J \quad \text{or} \quad \Delta \mathbf{f}^{\text{int}} = \mathbf{K}^M \Delta \mathbf{d}^M \tag{24}$$

In the above, $\mathbf{K}^C$ and $\mathbf{K}^M$ are tangent stiffness matrices given by

$$\mathbf{K}_{IJ}^C = \frac{\partial \mathbf{F}_I^{\text{int}}}{\partial \mathbf{u}_J} \qquad \mathbf{K}^C = \begin{bmatrix} \mathbf{K}_{11}^C & \mathbf{K}_{12}^C & \cdots & \mathbf{K}_{1n}^C \\ \mathbf{K}_{21}^C & \mathbf{K}_{22}^C & \cdots & \mathbf{K}_{2n}^C \\ \vdots & \vdots & \ddots & \vdots \\ \mathbf{K}_{n1}^C & \mathbf{K}_{n2}^C & \cdots & \mathbf{K}_{nn}^C \end{bmatrix} \tag{25}$$

$$\mathbf{K}_{IJ}^M = \frac{\partial \mathbf{f}_I^{\text{int}}}{\partial \mathbf{d}_J} \qquad \mathbf{K}^M = \begin{bmatrix} \mathbf{K}_{11}^M & \mathbf{K}_{12}^M & \cdots & \mathbf{K}_{1m}^M \\ \mathbf{K}_{21}^M & \mathbf{K}_{22}^M & \cdots & \mathbf{K}_{2m}^M \\ \vdots & \vdots & \ddots & \vdots \\ \mathbf{K}_{m1}^M & \mathbf{K}_{m2}^M & \cdots & \mathbf{K}_{mm}^M \end{bmatrix} \tag{26}$$

$$\mathbf{d}^C = \begin{Bmatrix} \mathbf{u}_1 \\ \mathbf{u}_2 \\ \vdots \\ \mathbf{u}_n \end{Bmatrix} \quad \mathbf{u}_I = \begin{Bmatrix} u_{xI} \\ u_{yI} \end{Bmatrix} \quad \mathbf{d}^M = \begin{Bmatrix} \mathbf{d}_1 \\ \mathbf{d}_2 \\ \vdots \\ \mathbf{d}_m \end{Bmatrix} \quad \mathbf{d}_I = \begin{Bmatrix} d_{xI} \\ d_{yI} \end{Bmatrix} \tag{27}$$

The Newton equations can then be written as

$$\begin{bmatrix} \mathbf{A}_{11} & \mathbf{A}_{12} & \mathbf{L}^{C^T} \\ \mathbf{A}_{21} & \mathbf{A}_{22} & \mathbf{L}^{M^T} \\ \mathbf{L}^C & \mathbf{L}^M & 0 \end{bmatrix} \begin{Bmatrix} \Delta\mathbf{d}^C \\ \Delta\mathbf{d}^M \\ \Delta\bar{\lambda} \end{Bmatrix} = \begin{Bmatrix} -\mathbf{r}^C \\ -\mathbf{r}^M \\ -\bar{\mathbf{g}} \end{Bmatrix} \tag{28}$$

The residuals in Eq. (25) can be expressed as:

$$\mathbf{r}^C = \mathbf{F}^{\text{int}} - \mathbf{F}^{ext} + \boldsymbol{\lambda}^T \mathbf{G}^C + p\mathbf{g}^T \mathbf{G}^C \tag{29}$$

$$\mathbf{r}^M = \mathbf{f}^{\text{int}} - \mathbf{f}^{\text{ext}} + \boldsymbol{\lambda}^T \mathbf{G}^M + p\mathbf{g}^T \mathbf{G}^M \tag{30}$$

$$\bar{\mathbf{g}} = \{\bar{g}_I\} = \left\{ \sum_K \Lambda_{IK} g_K \right\} \tag{31}$$

The other terms are:

$$\mathbf{A}_{11} = \mathbf{K}^C + \lambda_I \mathbf{H}_I^C + p(\mathbf{G}^{CT}\mathbf{G}^C + g_I \mathbf{H}_I^C) \tag{32}$$

$$\mathbf{A}_{12} = \lambda_I \mathbf{H}_I^{CM} + p(\mathbf{G}^{C^T}\mathbf{G}^M + g_I \mathbf{H}_I^{CM}) \tag{33}$$

$$\mathbf{A}_{21} = \lambda_I \mathbf{H}_I^{CM^T} + p(\mathbf{G}^{M^T}\mathbf{G}^C + g_I \mathbf{H}_I^{CM^T}) \tag{34}$$

$$\mathbf{A}_{22} = \mathbf{K}^M + \lambda_I \mathbf{H}_I^M + p(\mathbf{G}^{M^T}\mathbf{G}^M + g_I \mathbf{H}_I^M) \tag{35}$$

$$\lambda_I = \sum_K \Lambda_K(\mathbf{X}_I)\bar{\lambda}_K \tag{36}$$

$$\mathbf{L}^C = \left[\sum_L \Lambda_{IL} \frac{\partial g_L}{\partial d_i^C} \right] = \left[\sum_L \Lambda_{IL} \frac{\partial g_L}{\partial u_{kP}} \right] = \left[2\sum_L \Lambda_{IL} \left(\sum_K N_{KL} u_{kK} - d_{kL} \right) N_{PL} \right] \tag{37}$$

$$\mathbf{L}^M = \left[\sum_L \Lambda_{IL} \frac{\partial g_L}{\partial d_i^M} \right] = \left[\sum_L \Lambda_{IL} \frac{\partial g_L}{\partial d_{kP}} \right] = \left[-2\sum_L \Lambda_{IL} \left(\sum_K N_{KL} u_{kK} - d_{kL} \right) \delta_{PL} \right] \tag{38}$$

$$\mathbf{G}^C = \left[\frac{\partial g_I}{\partial d_i^C} \right] = \left[\frac{\partial g_I}{\partial u_{kP}} \right] = \left[2\left(\sum_K N_{KI} u_{kK} - d_{kI} \right) N_{PI} \right] \tag{39}$$

$$\mathbf{G}^M = \left[\frac{\partial g_I}{\partial d_i^M} \right] = \left[\frac{\partial g_I}{\partial d_{kP}} \right] = \left[-2\left(\sum_K N_{KI} u_{kK} - d_{kI} \right) \delta_{PI} \right] \tag{40}$$

$$\mathbf{H}_I^C = \left[H_{ij}^C \right]_I = \left[\frac{\partial^2 g_I}{\partial d_i^C \partial d_j^C} \right] = \left[\frac{\partial^2 g_I}{\partial u_{kP} \partial u_{lQ}} \right] = \left[2N_{PI} N_{QI} \delta_{kl} \right] \tag{41}$$

$$\mathbf{H}_I^M = \left[H_{ij}^M \right]_I = \left[\frac{\partial^2 g_I}{\partial d_i^M \partial d_j^M} \right] = \left[\frac{\partial^2 g_I}{\partial d_{kP} \partial d_{lQ}} \right] = \left[2\delta_{PI} \delta_{QI} \delta_{kl} \right] \tag{42}$$

$$\mathbf{H}_I^{CM} = \left[H_{ij}^{CM} \right]_I = \left[\frac{\partial^2 g_I}{\partial d_i^C \partial d_j^M} \right] = \left[\frac{\partial^2 g_I}{\partial u_{kP} \partial d_{lQ}} \right] = \left[-2N_{PI} \delta_{QI} \delta_{kl} \right] \tag{43}$$

4. COUPLING METHOD II: EDGE-TO-EDGE DECOMPOSITION

4.1. Coupling Model

The edge-to-edge decomposition coupling method we developed is shown in Fig. 4. As shown in Fig. 5, three types of particles are defined. Besides the nodes of the continuum domain and the atoms of the molecular domain, virtual atoms are defined to model the bond angle-bending for bonds between the continuum and the molecular domains. The virtual atoms are connected with the molecular domain by virtual bonds.

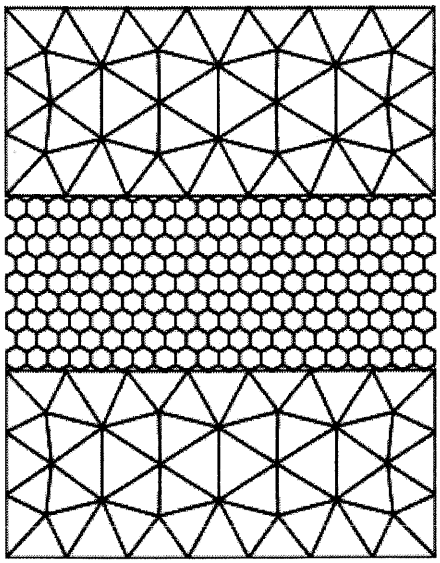

FIGURE 4. Edge-to-edge coupling.

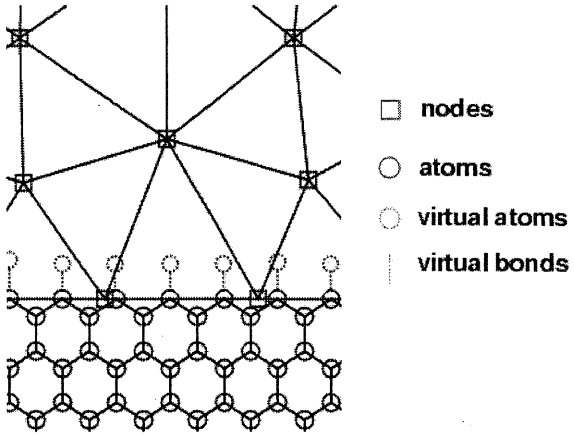

FIGURE 5. Definition of particles and bonds in edge-to-edge coupling.

The internal potential energy for the entire domain is given by

$$W^{\text{int}} = W^C + W^M = \int_{\Omega_0^C} \rho_0 w_C(\mathbf{F}) d\Omega_0^C + \frac{1}{2}\sum_I \sum_J w_M(\mathbf{x}_I, \mathbf{x}_J) \quad (44)$$

where W^M includes the bond angle-bending potential resulting from the bond angle change between the virtual bonds and adjacent bonds in the molecular domain; a virtual bond fg is shown in Fig. 6.

The motion of the virtual atom f will depend on the nodes of element ABC that contains this virtual atom. Therefore, we can express $\mathbf{u}_f$ in terms of $\mathbf{u}_I$ by

$$\mathbf{u}_f(\mathbf{X}, t) = \sum_I N_I(\mathbf{X})\mathbf{u}_I(t) \qquad I = A, B, C \quad (45)$$

It should be noted here that the stretching energy of virtual bond fg is already included in the potential of the continuum, W^C. Therefore, the only potential energy that the virtual bond, fg, contributes to the total potential is the bond angle-bending energy caused by the angle change of this virtual bond with its adjacent bonds; this is included in W^M. It is given by

$$W_f^{interface} = E_{angle}(\theta_{fge}) + E_{angle}(\theta_{fgd}) \quad (46)$$

In this coupling method, the same constraints are used on the interface as in Eq. (13). $\mathbf{u}(\mathbf{X}_K)$ can also be given by the linear finite element approximation as shown in Fig. 7:

$$\mathbf{u}(\mathbf{X}_K) = N_{1K}\mathbf{u}_1 + N_{2K}\mathbf{u}_2 \quad (47)$$

The Lagrange multiplier method and the augmented Lagrangian method can be applied as before. The Lagrange

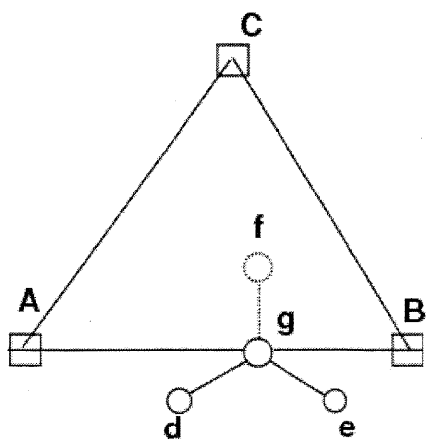

FIGURE 6. Virtual atom and bond.

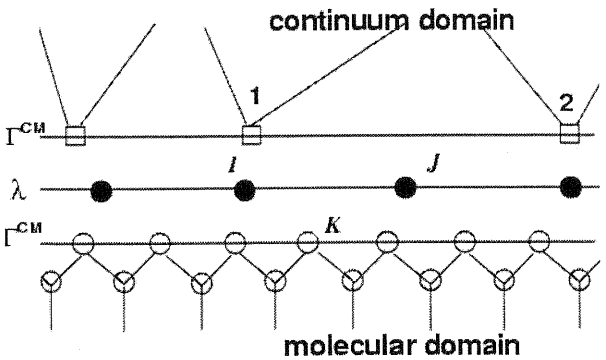

FIGURE 7. Constraints on interface between two domains.

multiplier field can be viewed as a multisegment line attached to the interface Γ^{CM}, and λ_K is given by the linear finite element approximation where the segment IJ is mapped to the parent [0,1] element. Therefore,

$$\lambda_K = \Lambda_{IK}\bar{\lambda}_I + \Lambda_{JK}\bar{\lambda}_J = (1-\xi_K)\bar{\lambda}_I + \xi_K\bar{\lambda}_J \tag{48}$$

The potential function for the augmented Lagrangian method for this coupling model is

$$W_{AL} = W^{\text{int}} - W^{\text{ext}} + \boldsymbol{\lambda}^T\mathbf{g} + \frac{1}{2}p\mathbf{g}^T\mathbf{g} \tag{49}$$

where W^{int} is given by Eq. (44), and the external potential W^{ext} can be written as

$$W^{\text{ext}} = \mathbf{F}_I^{\text{ext}} \cdot \mathbf{u}_I + \sum_I \mathbf{f}_I^{\text{ext}} \cdot \mathbf{d}_I \tag{50}$$

4.2. Discrete Equations

A stable equilibrium state can be obtained when the first derivatives of Eq. (49) with respect to $\mathbf{u}$ (or $\mathbf{d}$) and $\bar{\lambda}$ vanish, so

$$dW_{AL} = dW^{\text{int}} - dW^{ext} + d(\boldsymbol{\lambda}^T\mathbf{g}) + p\mathbf{g}^T d\mathbf{g}$$
$$= d\mathbf{u}^T\left(\gamma^{\text{int}} - \gamma^{ext} + \boldsymbol{\lambda}^T\frac{\partial\mathbf{g}}{\partial\mathbf{u}} + p\mathbf{g}^T\frac{\partial\mathbf{g}}{\partial\mathbf{u}}\right) + d\lambda^T\mathbf{g} = 0 \tag{51}$$

where $d\lambda_I = \Lambda_{KI}d\bar{\lambda}_K$.

The residuals are

$$\gamma^{\text{int}} = \begin{Bmatrix}\mathbf{F}^{\text{int}}\\ \mathbf{f}^{\text{int}}\end{Bmatrix} \qquad \gamma^{\text{ext}} = \begin{Bmatrix}\mathbf{F}^{\text{ext}}\\ \mathbf{f}^{\text{ext}}\end{Bmatrix} \tag{52}$$

and

$$\mathbf{F}_J^{\text{int}} = \int_{\Omega_0^C}\rho_0\frac{\partial w_C(\mathbf{F})}{\partial\mathbf{u}_J}d\Omega_0^C$$
$$\mathbf{f}_J^{\text{int}} = \frac{1}{2}\sum_I\sum_J\frac{\partial w_M(\mathbf{x}_I,\mathbf{x}_J)}{\partial\mathbf{d}_J} \tag{53}$$

The linearized model for this edge-to-edge decomposition coupling method can also be derived as was done for the overlapping domain decomposition coupling model.

5. EXAMPLES

5.1. Bending of Graphite Sheet

A 1-atom-thick graphite sheet is bent by rotating its ends in opposite directions. The dimensions of the sheet are l_x = 4.82 nm and l_y = 24.88 nm, and it contains 4,920 atoms. The potential function used here is the modified Morse potential [1]:

$$w_M(\mathbf{x}_I,\mathbf{x}_J) = E_{stretch} + E_{angle}$$

$$E_{stretch} = D_e\{[1-e^{-\beta(r-r_0)}]^2 - 1\}$$

$$E_{angle} = \frac{1}{2}k_\theta(\theta-\theta_0)^2[1+k_{sextile}(\theta-\theta_0)^4] \tag{54}$$

where $E_{stretch}$ is the bond energy caused by bond stretch, while E_{angle} is the bond energy caused by bond angle bending, r is the length of the bond, and θ is the current angle of the adjacent bond, a standard deformation measure in molecular mechanics. The parameters are

$$r_0 = 1.39\times10^{-10}m \qquad D_e = 6.03105\times10^{-19}N\cdot m$$
$$\beta = 2.625\times10^{10}m^{-1} \qquad \theta_0 = 2.094rad$$
$$k_\theta = 0.9\times10^{-18}N\cdot m/rad^2 \qquad k_{sextile} = 0.754rad^{-4}$$

Figure 8a shows the deformed configuration for the bending angle θ = 25° by molecular mechanics. The deformed configurations from the two coupling methods are shown in Figs. 8b and 8c, respectively. We can see that the configurations are nearly identical.

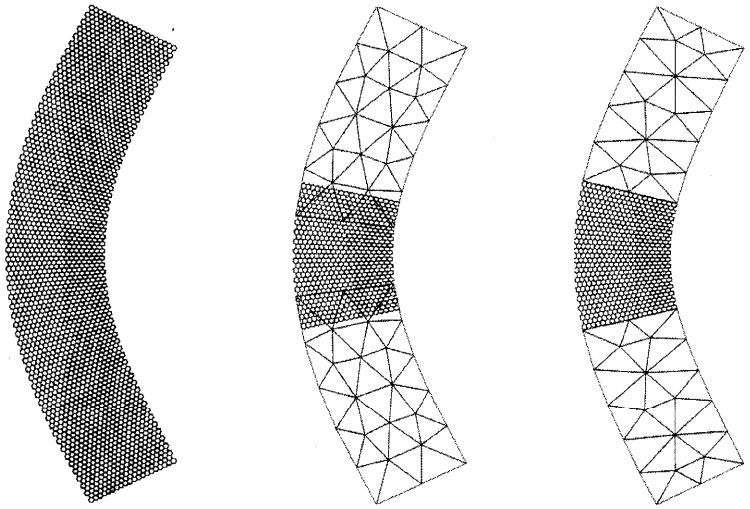

(a) molecular mechanics (b) overlapping coupling (c) edge-to-edge coupling

FIGURE 8. Comparison of deformed configuration of bending graphite sheet.

We study the convergence of the coupling by using the l_2 error in displacement for the coupling methods. The error in displacement is defined as:

$$error_{l_2} = \frac{l_2[\mathbf{u}_I - \mathbf{u}^C(x_I)]}{l_2[\mathbf{u}^C(x_I)]} \tag{55}$$

where

$$l_2(\mathbf{u}) = \left(\sum_{I=1}^{n} \mathbf{u}_I^2 \Delta V_I \right)$$

where ΔV_I is the volume of atom I (it is constant here), $\mathbf{u}_I$ are the displacements of atoms from a complete atomistic model, and $\mathbf{u}^C(x_I)$ are the displacements of the same atoms from the coupling method. Note that only the positions of the molecules in the coupling methods are included in the error measure (55). The results are shown in Fig. 9. We can see that the edge-to-edge coupling method gives less error in the displacements than the overlapping coupling method if the same element sizes are used. However, the overlapping coupling method has an advantage over the edge-to-edge coupling because virtual atoms or bonds are not required.

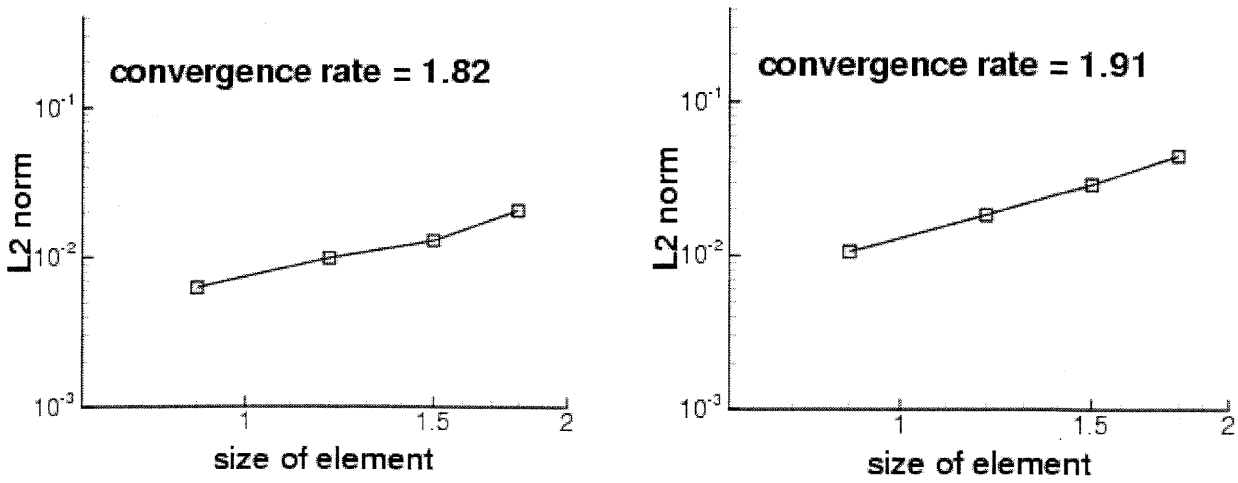

(a) edge-to-edge decomposition (b) overlapping domain decomposition

FIGURE 9. Accuracy of coupling in terms of norm in displacement of molecular.

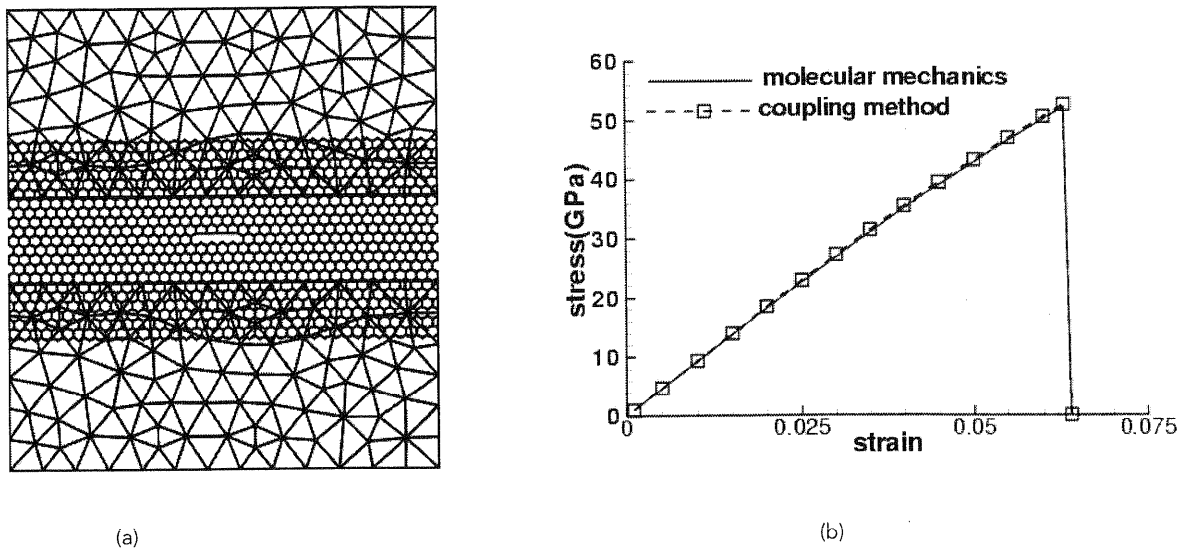

(a) (b)

FIGURE 10. Comparison between coupling method and molecular mechanics.

5.2. Fracture of Graphite Sheet

A graphite sheet 10.286nm long and 9.6302nm wide is studied in this example. There are 4,050 atoms in this graphite sheet, with a crack in the center from a 4-atom defect. In the overlapping domain decomposition coupling method, the molecular domain is in the middle of the graphite sheet, and two continuum domains are on the two sides of the molecular domain. It contains 210 elements and 1,782 atoms, as shown in Fig. 10a.

The displacement is prescribed on the upper end of the graphite sheet, and the lower end is fixed. The stress–strain curves are shown in Fig. 10b for the complete molecular mechanics model and the overlapping coupling method. Strain is denoted by ε and is defined by $\varepsilon = [(l - l_0) / l_0]$, where l_0 is the equilibrium (initial) length and l is the current length of the bond (i.e., the distance between nuclei). Stress is calculated by $\sigma = (F/ht)$, where F is the summation of the interatomic force of the atoms on the upper boundary, h is the width of the graphite sheet, and t is the thickness of the graphite sheet, which is taken to be 0.34 nm. From Fig. 10b we can see that both computed stresses exhibit a sudden drop to zero at failure, so the fracture can be considered brittle.

5.3. Bending of Nanotube

A [10,0] nanotube 8.4 nm long is bent here. Both ends of the nanotube are rotated in opposite directions. The modified Morse potential is used, as described in Eq. (54). The overlapping domain decomposition coupling method is used to compare with a complete molecular mechanics model. Figure 11 shows the deformed configuration when the bending angle is 30°, and Fig. 12 shows the comparison of potential energies. The small difference of potential

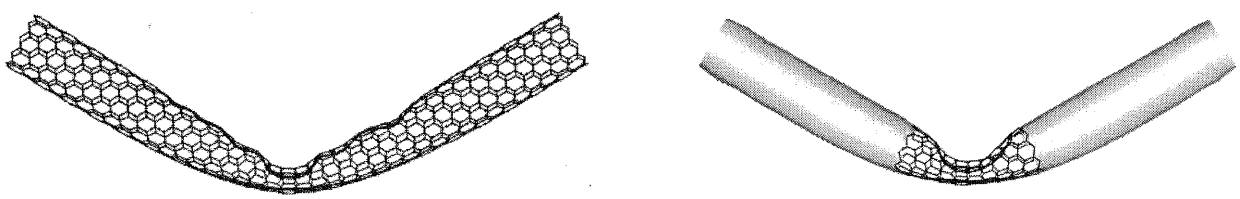

(a) molecular mechanics (b) overlapping coupling method

FIGURE 11. Comparison of molecular and coupled model results for bending of nanotube.

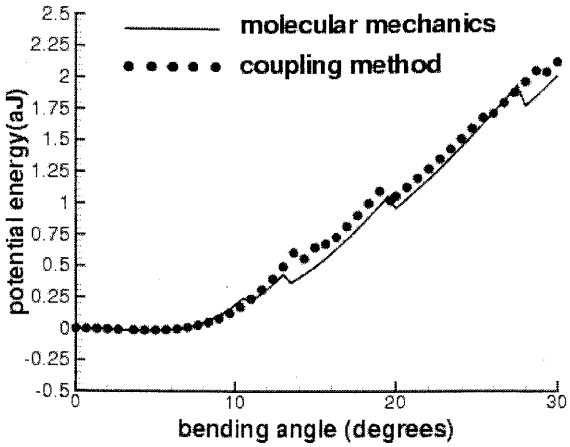

FIGURE 12. Comparison of potential between molecular mechanics and coupling method.

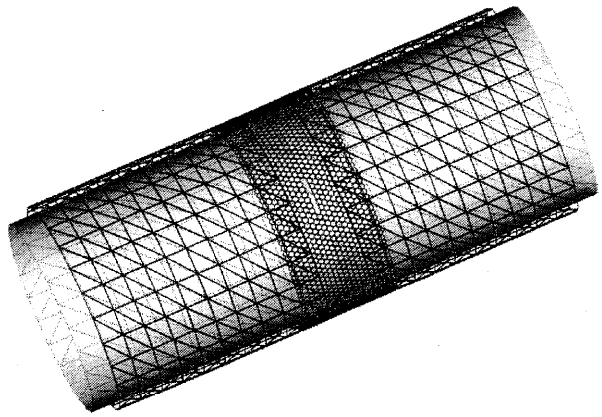

FIGURE 13. Nanotube model for fracture study by overlapping coupling method.

between molecular mechanics and the coupling method is due to the fact that the continuum model didn't catch the slight kinks that occur in the molecular mechanics model. For large nanotubes, the coupling method is in good agreement with molecular mechanics.

5.4. Nanotube Fracture

An example of the type of model we have used for fracture studies is shown in Fig. 13. It consists of two nested nanotubes that interact by van der Waals forces. The molecular model is used only in a small subdomain outside the nanotube, around a defect incorporated in the model. The outside nanotube is a [120,0] nanotube, its radius is 4.6 nm, and its length is 21.2nm. The modified Morse potential [1] was used. The load was applied only to the outside tube. These two nanotubes contain 46,200 atoms, so a complete molecular mechanics simulation would be very expensive.

Figure 14 shows the failure stresses for various defects as compared to the experiments of Yu et al. [11]; the results for smaller models have been reported by Belytschko et al. [12] and are almost identical. It is interesting to observe that the model with defects agrees much more closely with the experiments than does a perfect nanotube.

6. CONCLUSION

Two kinds of coupling methods for continuum model and molecular model have been developed: the overlapping domain decomposition method and the edge-to-edge decomposition method. Both methods were shown to be quite accurate for moderate and large deformation problems. The linearized models were also given for these two coupling methods when they are applied in Newton methods. These coupling methods can be used to study the behavior of large nanotubes, especially for nanotube fracture. They also can be extended to the finite element method coupled with particle methods.

ACKNOWLEDGMENT

We gratefully acknowledge the grant support of NASA University Research, Engineering, and Technology Institute on Bio Inspired Materials (BIMat), award No. NCC-1-02037.

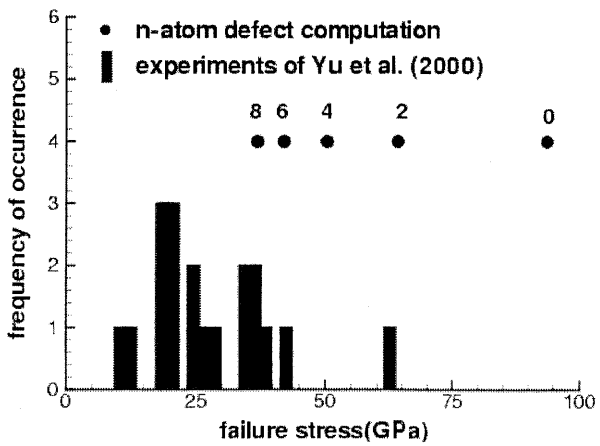

FIGURE 14. Experimental failure stresses [11] as compared to computation.

REFERENCES

1. Belytschko, T., Xiao, S. P., Schatz, G. C., and Ruoff, R. Atomistic simulations for nanotube fracture. *Phys. Rev. B.* 65:235430, 2002.
2. Arroyo, M. and Belytschko, T. An atomistic-based finite deformation membrane for single layer crystalline films. *J. Mech. Phys. Solids* 50:1941–1977, 2002.
3. Dryja, M. A finite element-capacitance method for elliptic problems on regions partitioned into subregions. *Numer. Math.* 44:153–168, 1984.
4. Quarteroni, A. and Valli, A. *Domain Decomposition Methods for Partial Differential Equations.* Clarendon Press, Oxford–New York, 1999.
5. Abraham, F. F., Broughton, J. Q., Bernstein, N., and Kaxiras, E. Spanning the length scales in dynamic simulation. *Comput. Phys.* 12(6):538–546, 1998.
6. Bank, R. E., Jimack, P. K., Nadeem, S. A., and Nepomnyaschikh, S. V. A weakly overlapping domain decomposition preconditioner for the finite element solution of elliptic partial differential equations. *SIAM J. Sci. Comput.* 23(6):1817–1841, 2002.
7. Zhu, Z. Q., Lu, X. B., and Li, J. A study of domain decomposition and parallel computation. *ACTA. Mech.* 150(3–4): 219–235, 2001.
8. Elleity, W. M., Al-Gahtani, H. J., and El-Gebeily, M. Iterative coupling of BE and FE methods in elastostatics. *Eng. Anal. Bound. Elem.* 25(8):685–695, 2001.
9. Rischmuller, V., Haas M., Kurz, S., and Rucker, W. M. 3D transient analysis of electromechanical devices using parallel BEM coupled to FEM. *IEEE T. Mag.* 36(4): 1360–1363, 2000.
10. Belytschko, T., Liu, W. K., and Moran, B., *Nonlinear Finite Elements for Continua and Structures.* Wiley, New York, 2000.
11. Yu, M. F., Lourie, O., Dyer, M. J., Moloni, K., Kelly, T. F., and Ruoff, R. S. Strength and breaking mechanism of multiwalled ccarbon nanotubes under tensile load. *Science* 287:637–640, 2000.
12. Belytschko, T., Xiao, S. P., and Ruoff, R. Effects of defects on the strength of nanotubes: experimental–computational comparisons. arXiv.org e-Print archive, physics/0205090, Los Alamos.